Pilot-scale in situ water electrolyzer with an improved fluid flow and modified electrodes for upscaling hybrid biological–inorganic systems

Givirovskiy Georgy, Ruuskanen Vesa, Kokkonen Petteri, Karvinen Aku, Givirovskaia Daria, Repo Eveliina, Ahola Jero

DOI: 10.1016/j.jclepro.2021.128001

Journal of Cleaner Production 314 (2021) 128001

Contents lists available at ScienceDirect

Journal of Cleaner Production

journal homepage: www.elsevier.com/locate/jclepro

Pilot-scale in situ water electrolyzer with an improved fluid flow and modified electrodes for upscaling hybrid biological–inorganic systems

Georgy Givirovskiy [a,*], Vesa Ruuskanen [a], Petteri Kokkonen [b], Aku Karvinen [b], Daria Givirovskaia [a], Eveliina Repo [a], Jero Ahola [a]

[a] LUT University, P.O. Box 20, FI-53851, Lappeenranta, Finland
[b] VTT Technical Research Centre of Finland Ltd, P.O. Box 1000, 02044, VTT, Finland

ARTICLE INFO

Handling editor: Cecilia Maria Villas Bôas de Almeida

Keywords:
In situ water electrolysis
Electrolyzer stack design
Hybrid biological–inorganic system
Electrocatalyst
pH-neutral conditions
Environmental sustainability

ABSTRACT

Anthropogenic emissions of CO_2 and other greenhouse gases have increased since the pre-industrial era, driven largely by economic and population growth, and are now higher than ever. In this scope, hybrid biological–inorganic systems represent a sustainable and versatile chemical synthesis platform using CO_2 as a feedstock which realizes the idea of 'Cleaner Production'. Practical implementation of hybrid biological–inorganic systems for the production of value-added chemical products requires development of scalable and robust electrobioreactors with a high energy efficiency and an adequate size. This work reports an in situ water electrolyzer stack design as part of an electrobioreactor system required for the pilot-scale operation of the hybrid biological–inorganic process approaching the aforementioned requirements. The electrolyzer is designed by applying fluid dynamics simulation tools to model the electrolyte flow. The design takes into consideration the problem of leakage currents, reported in the previous works, which is tackled by applying an electrically insulating coating. Different electrode surface modification approaches, such as coating with electrocatalysts and etching, are used to further enhance the performance and energy efficiency of the electrolyzer. The performance of the electrolyzer stack was evaluated in a pH-neutral solution required for the hybrid biological–inorganic processes. The in situ water electrolyzer developed in this study showed a high Faraday efficiency close to 90% and acceptable specific energy consumption below 90 kWh kg_{H2}^{-1}. The obtained energy-efficiency values are the highest reported for similar applications with a similar scale which emphasizes the successful design of the in situ water electrolyzer stack. All data collected during experimental work might be applied to further investigation, simulation, and optimization of electrobioreactors operating at neutral pH. Overall, the results achieved in this study are promising and represent a crucial step toward the industrial implementation of hybrid biological–inorganic systems.

1. Introduction

Technologies capable of combining sustainable energy generation and production of valuable products are needed to adjust the focus from a fossil-based economy to a renewable and circular economy and to tackle environmental pollution (Nocera and Nash, 2006; Geissdoerfer et al., 2017). In this context, hybrid biological–inorganic (HBI) systems coupling the advantages of biological components and electrochemical techniques provide a sustainable and efficient chemical synthesis platform. A variety of high-value products, such as biomass, polymers, and alcohols, can be synthesized by using hybrid technology. The operating principle of HBI systems is based on the utilization of specific autotrophic microorganisms interfaced to biocompatible electrodes in systems with integrated water electrolysis. These biocompatible electrodes or catalysts are, in turn, used for the conversion of electrical energy into H_2 or energetic reducing equivalents, subsequently used by microbes as an energy source for assimilation of CO_2 and building of new carbonaceous compounds. In this regard, HBI systems might potentially play a significant role in storing energy from intermittent energy sources and also provide a reliable mechanism for fixing CO_2 – the annual anthropogenic emissions reaching 32 billion metric tons (Nangle et al., 2017).

The HBI processes circumvent many of the challenges inherent to purely chemical conversion of CO_2 (Szczygieł and Kułażyński, 2020;

* Corresponding author.
E-mail addresses: georgy.givirovskiy@lut.fi, georgy_givirovskiy@mail.ru (G. Givirovskiy).

https://doi.org/10.1016/j.jclepro.2021.128001
Received 26 February 2021; Received in revised form 7 June 2021; Accepted 16 June 2021
Available online 22 June 2021

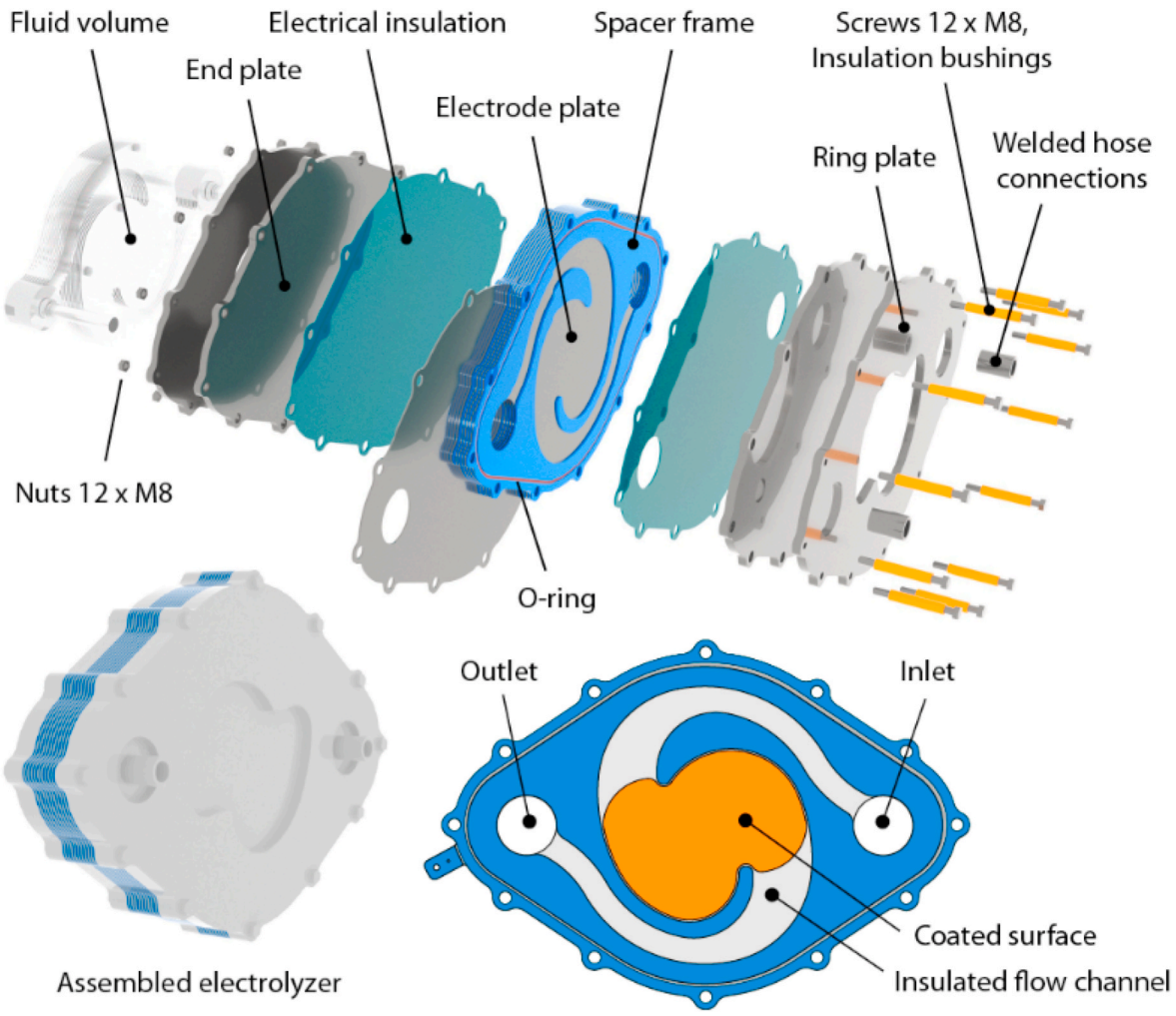

Fig. 1. In situ water electrolysis stack with ten cells in series. An exploded view, assembly, and the coated surfaces of the electrode plate. The spacer frame acts as the flow guide and separates the electrode plates at the desired distance. The flow channels, bolts, and end plates are insulated to reduce the leakage currents. The coated active surface area in the electrolysis process is shown with orange color.

Nieminen et al., 2018), among which are selectivity problems between organic products of a similar thermodynamic potential, difficulties of performing multielectron reductions for C–C bond formation, slow CO_2 reduction rates, and gas transfer limitations caused by the low solubility of the main reactant gases. After the phenomenological and proof-of-concept discovery of the HBI process, the scientific focus has shifted toward the objectives of enhanced energy efficiency, product selectivity, process robustness, and upscaling (Nangle et al., 2017).

Practical implementation and upscaling of the HBI technology is, to a great extent, dependent on the successful solution of the challenges identified in the initial phase. Important scientific tasks, revealed in the first stage, include promotion of the intimate association of electrotrophs and high surface area electrodes, study of mechanism of electron transfer from electrode to bacterium and avoidance of toxic byproducts synthesis (Nangle et al., 2017). The attempts to solve the later problem included the development of selective electrocatalysts that kinetically favor H_2 production instead of reactive oxygen species (ROS) generation (Liu et al., 2016). In this regard, the key research directions cover, but are not limited to, the following aspects: development of stable microbial cultures or microbiomes enabling fast CO_2 conversion rates under aerobic growth conditions, successful implementation of advances in bioreactor and process designs, as well as integration of innovative material structures (Osadolor et al., 2014; Alattar and Bazhin, 2020).

The upscaling of an HBI system is closely associated with the development of a robust, efficient, and ergonomic reactor design with in-situ electrolysis of the cultivation medium (De Francesco and Costamagna, 2004; Wrana et al., 2010). For this purpose, stackable reactor structures, widely used in industrial electrolysis (Bhandari et al., 2014) and dialysis applications, represent a viable technological option capable of achieving targeted volumes by simply increasing the number of stacked units (Krieg et al., 2014). Furthermore, using a stacked reactor for in situ electrolysis has multiple advantages, among which are, for instance, the improved power output and current generation, avoidance of ohmic losses and edge effects, homogeneous current distribution over the reaction volume, and ease of characterization of the overall performance by analyzing the performance of individual cells (Givirovskiy et al., 2019).

There are a few applications of stacks for HBI processes available in the literature, with most of the research concentrating on single electrolytic cells immersed in the cultivation medium (Torella et al., 2015; Liu et al., 2018). Nevertheless, this technology could presumably mitigate many of the existing problems attributed to HBI systems, such as the low conductivity of the cultivation medium, an increase in the ohmic losses, current density limitations set by the microorganisms (Zhang et al., 2020), and the requirements for a design with an acceptable electrode surface-to-volume ratio. Moreover, a substantial improvement in performance can be reached by using coatings of electrode surfaces (Givirovskiy et al., 2020), which, at the same time, tackle biocompatibility issues (Liu et al., 2016).

In this paper, our research group proposes a novel stack structure

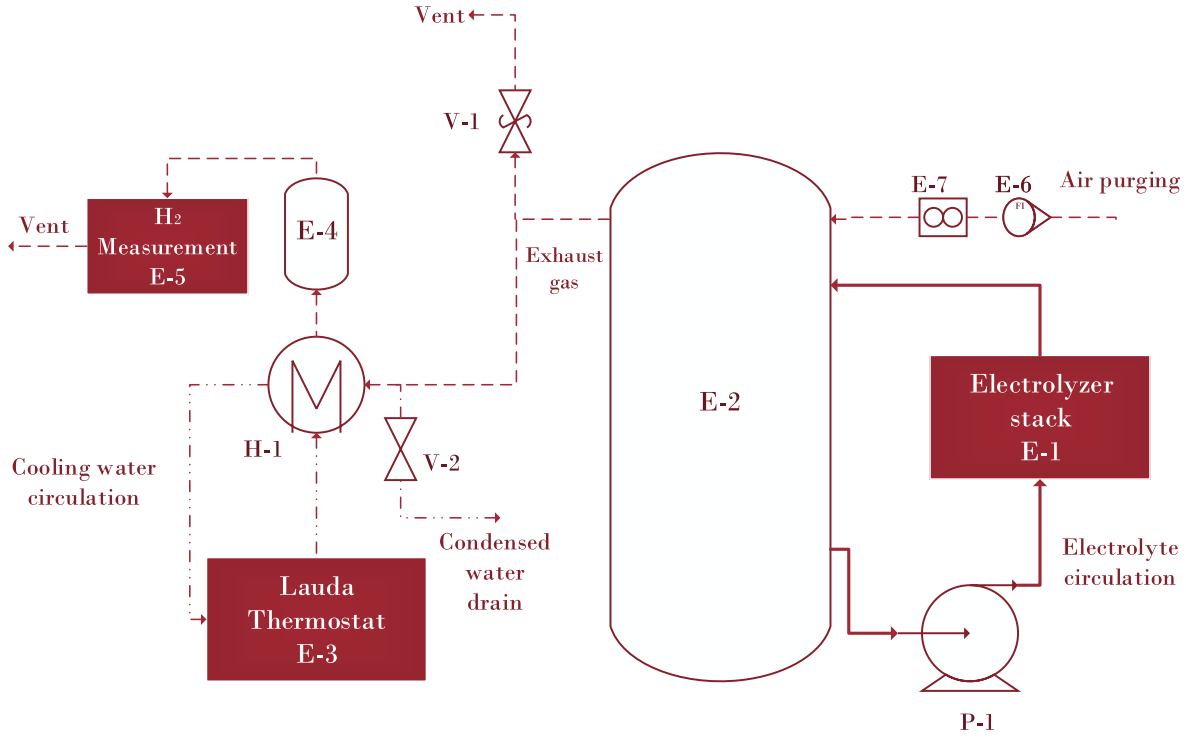

Fig. 2. Process flow diagram of the experimental setup.

design for in situ water electrolysis in HBI systems. The stack is anticipated to increase the hydrogen production rate and the energy efficiency in comparison with the previous versions (Givirovskiy et al., 2019; Ruuskanen et al., 2021). The performance of the stack is experimentally studied, and fluid dynamics simulations are used to design and evaluate the fluid flow.

2. Materials and methods

The following section provides insight into the materials and methods used in this study. First, the in situ water electrolyzer stack design is described in detail followed by the description of the experimental setup used for water electrolysis tests. Thereafter, details related to the preparation of electrocatalysts are presented complemented with the surface characterization techniques used in this study. Eventually, electrochemical methods and fundamental equations describing water electrolysis are given for the readers.

2.1. Materials

Commercially available analytical grade chemicals were used as received without further purification. The stack plates were manufactured from duplex stainless steel 1.4462, purchased from Karose Oy. The following compositional summary of the selected steel material can be found from the material data sheet: Fe 64–72% / Cr 21–23% / Ni 4.5–6.5% / Mo 2.5–3.5% / N 0.08–0.2% (impurities: Mn < 2%, Si < 1%, C < 0.03%, P < 0.03%, S < 0.02%). The insulating Teflon coating for the stack plates was acquired from ATV-Pintakäsittely Oy.

2.2. Description of the in situ water electrolyzer stack design

An improved stacked electrolyzer device was designed based on experiences gained from the test runs with the electrolyzer devices presented in (Givirovskiy et al., 2019; Ruuskanen et al., 2021). Different sources of uncertainty related to the functionality of the electrolyzer device were identified, and countermeasures were devised in the electrolyzer design. The main uncertainties were (i) signs of local erosion or corrosion; (ii) occurrence of leakage currents; (iii) variation in the contact conditions between the spacers and the electrode plates; and (iv) variation in the distance between the electrode plates, which may cause concentration of the electrical current density. The main design changes compared with the previous electrolyzer devices (Givirovskiy et al., 2019; Ruuskanen et al., 2021) were (i) arrangement of the fluid flow through electrically insulated flow channels to decrease the stray currents; (ii) the use of a parallel flow arrangement for even flow velocity distribution; and (iii) a decrease in the pressure drop. The electrolyzer device, shown in Fig. 1, comprises a stack of electrode plates separated by spacer frames and sealed by o-rings. The spacer frames also act as flow guides. The stainless steel end plates carry the pressure load. The stack is assembled with 12 M8 bolts. The ring plate under the bolts provides even distribution of the bolt preload to the spacer frames and seals to avoid leaking. The electrical connections were laser cut to the electrode plates to monitor the electrical current and potential separately at each electrode.

The corrosion resistance of the electrode plates was improved by using duplex stainless steel 1.4462 with the pitting resistance equivalent (PRE) number of 35.1 in comparison with the stainless steel AISI 316L with the PRE number of 24.4 used in the previous electrolyzer (Ruuskanen et al., 2021). In addition, the risk of cavitation was decreased by avoiding abrupt changes in the flow direction by using a parallel flow arrangement. The conditions favoring cavitation were considered to increase the risk of corrosion by local erosion and oxygen present in the process. The rolled surfaces of the duplex steel electrode plates were ground at grit 600 by a roll grinder to provide a roughened surface for the basis of the coating.

To minimize the leakage currents that reduce the Faraday efficiency of the electrolyzer stack, 100 μm Teflon coating was applied. The resistance of the leakage current path through the electrolyte flow channels was maximized by completely coating the electrode plate, only excluding the active areas indicated by orange color in Fig. 1. Special attention was paid to the coating quality in the axial inlet and outlet flow channel areas. Further, the length of the insulated flow channels

between the electrode plates was maximized despite the increased need for electrode plate material.

In the improved electrolyzer device, the fluid is fed by a centrifugal pump to the inlet manifold, from which the fluid flows parallel between the electrodes, and further to the outlet manifold. The distance between the electrode plates is set to 2 mm, compared with the previous 3 mm, to increase the efficiency of the electrochemical process by decreasing the ohmic losses caused by the resistivity of the pH-neutral electrolyte. The active cell area is 239 cm^2. The distance is defined by the thickness of the spacer frame. The relatively small distance between the electrodes tends to keep the flow laminar, and therefore, mixing by turbulence was not applicable in the current design. The electrolyzer device was designed for lab-scale test runs, but the scalability to the industrial scale was considered in the choices throughout the design process. The stack arrangement enables linear scaling of the process by varying the number of electrode pairs. The laminar flow condition and the low-pressure drop at the parallel flow arrangement allow a rather linear scalability also by variation of the diameter, as the small distance between the electrodes tends to keep the flow laminar despite the change in the electrode plate diameter. To ensure the flatness of the electrode plates on the industrial scale, intermediate spacers can be used to support the electrode plates from bending. Further, intermediate spacers can also be used as flow guides.

2.3. Experimental setup

Fig. 2 illustrates the flow diagram of the experimental setup used for the electrolysis tests, consisting of (i) an electrolyzer stack (E-1); (ii) a constant-flow water circulation pump (P-1); (iii) a plastic vessel for the electrolyte input and output (E-2); (iv) an exhaust gas analysis equipment (E-5); and (v) control automation.

A Grundfos Alpha2 25–60 household hot water circulation pump (P-1) with an integrated frequency converter was used for pumping of the electrolyte. In order to avoid H_2 accumulation in the headspace of the plastic vessel (E-2), flushing with air was applied. The flush air flow was controlled with a manual pressure regulator (E-7) and a needle valve and measured with a MASS-VIEW MV-104 mass flow meter (E-6). The H_2 concentration in the exhaust gas was analyzed using an SRS BGA244 binary gas analyzer (E-5) equipped with a two-stage drying solution based on a water-condensing plate heat exchanger (H-1) followed by a silica gel tank (E-4) to prevent moisture ingress from the gas flow into the gas analyzer. Water for the plate heat exchanger was cooled down to 1 °C by a Lauda circulation thermostat (E-3). The electrolyzer stack current was supplied and measured by a GAMRY reference 3000 potentiostat and a Reference 30k booster. A Hioki PW6001 power analyzer with a Hioki CT6862-05 current probe was used for the verification of the measurements. The measurement system control automation of the pilot setup was implemented in a LabVIEW environment. All the data were stored online with a 100 ms interval to the LUT measurement database, which can be accessed with the Grafana data observation platform.

2.4. Modification of the electrolyzer stack plates

The procedure for catalyst fabrication was adopted from previous reports (Kanan and Nocera, 2008; Xing et al., 2016). Electrodeposition was the main method used for the coating preparation of the catalysts. Prior to deposition, the active area of each electrolyzer stack plate was polished with sandpaper, cleaned in 2M HCL to remove the oxide layer, and rinsed with acetone and distilled deionized water to remove possible surface contaminants. Then, the plates were dried in ambient air before further use.

To obtain the solution for the electrodeposition of Co–Pi, 0.5 mM of $Co(NO_3)_2{\cdot}6H_2O$ was added to the phosphate buffer solution (PBS), which was prepared by mixing 0.1 M KH_2PO_4 and 0.1 M K_2HPO_4. The solution for CoFe–P was prepared by dissolving 0.0375 M $CoSO_4 \cdot 7H_2O$, 0.0125 M $FeSO_4 \cdot 7H_2O$, 0.5 M $NaH_2PO_2 \cdot H_2O$, and 0.1 M NaOAc · $3H_2O$.

The Co–Pi catalyst coating was prepared in situ by cyclic voltammetry using the anodic electrodeposition strategy at a scan rate of 5 mV/s in a potential range from 1.7 V to 2.2 V for 4 h. For the deposition of the CoFe–P coating, the cathodic electrodeposition strategy using the chronoamperometry mode was applied at a constant voltage of −2.6 V for 45 min.

The etching solution contained approximately two portions of 30% H_2O_2 solution and one portion of 35% HCl solution. The etchant was poured onto the active surface of each electrolyzer plate with a syringe and left for 30 min. Subsequently, the etchant was gently removed by using a paper towel, and the surfaces were rinsed with deionized water. Teflon was protected by applying adhesive tape.

All solutions were prepared in ultrapure doubly distilled water obtained from a PURELAB flex system. After deposition, all plates were again gently rinsed with distilled deionized water and dried in ambient air before the electrochemical measurement tests.

2.5. SEM and XRD characterization

A Hitachi S–3400N field-emission scanning electron microscope (SEM) equipped with energy-dispersive X-ray spectroscopy (EDX) measurement was used to examine the surface morphologies and the compositional distribution of the elements of the fabricated catalysts. SEM images were obtained by operating the microscope at 10 kV and 20 mA using a UDV (secondary electron detector) and a BSE (backscatter electron detector). X-ray diffraction (XRD) analysis performed with a Bruker D8 Advance X-ray diffractometer was used to analyze the crystal structure of the studied electrocatalysts. XRD patterns were obtained at 40 kV, 30 mA with Cu Kα-type radiation.

2.6. Electrochemical measurements

All the electrochemical measurements were conducted with a potentiostat and booster by Gamry Instruments, the USA. The electrolyzer was connected by using a two-electrode configuration to measure the voltage drop across the whole device. A PBS solution, which was prepared by mixing 0.1 M KH_2PO_4 and 0.1 M K_2HPO_4, was used as an electrolyte for all the electrochemical measurements. Polarization curves were obtained by linear sweep voltammetry (LSV) at a scan rate of 20 mV s^{-1}.

2.7. Performance evaluation

There are several crucial parameters describing the water electrolysis process. The minimum thermodynamic potential required for water electrolysis, called reversible voltage, is 1.23 V in standard ambient conditions. Without auxiliary heat, the required minimum voltage is higher and dependent on the electrolysis conditions (e.g., 1.48 V in standard ambient conditions). From the perspective of energy efficiency, the voltage driving the electrolysis should thus be kept as low as possible. The actual voltage required to drive the electrolysis is higher because of overvoltages (i.e. voltage losses) caused by the impedance between the electrodes and the activation reactions. Hence, the overall cell voltage is the sum of different overvoltages (overpotentials) presented in the following equation

$$U_{cell} = U_{rev} + U_{ohm} + U_{act} + U_{con}, \quad (1)$$

where U_{cell} is the cell voltage, U_{rev} is the reversible open circuit voltage, U_{ohm} is the overvoltage caused by ohmic losses in the cell elements, U_{act} is the activation overvoltage caused by electrode kinetics, and U_{con} is the concentration overvoltage caused by the mass transport processes (Ursúa et al., 2012).

Cell voltages are typically well above the thermoneutral voltage

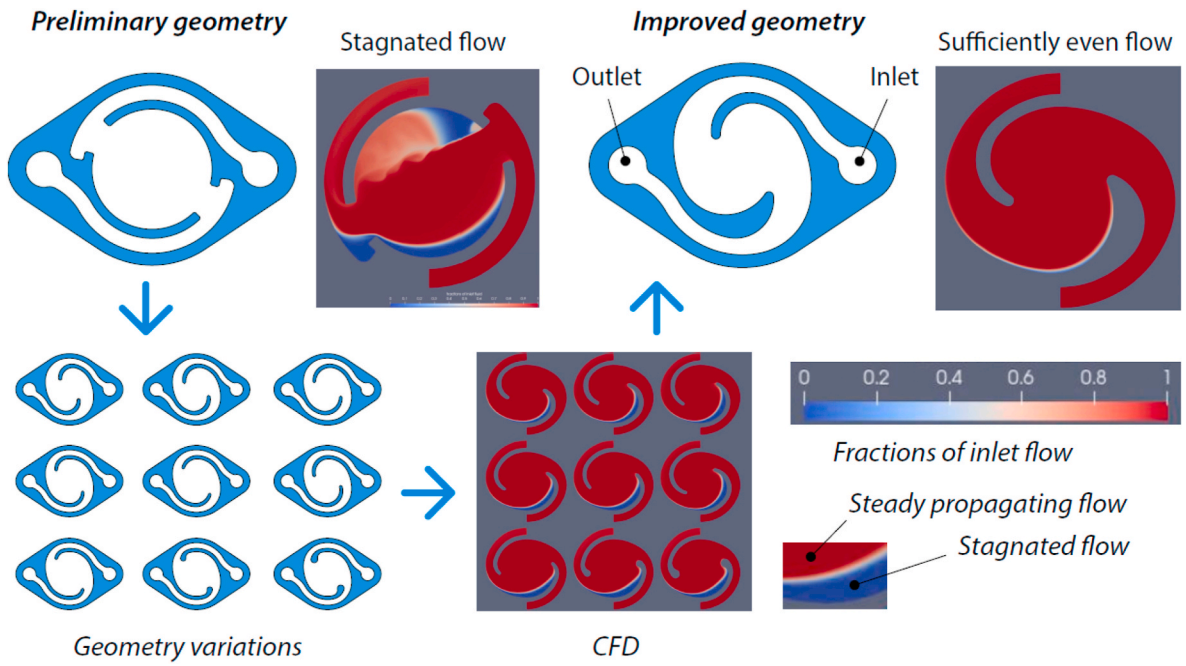

Fig. 3. CFD-based design of the flow guide.

1.48 V. Voltage efficiency can be defined by the stack voltage and the thermoneutral voltage

$$\eta_U = \frac{U_{tn} N_{cell}}{U}, \tag{2}$$

where U_{tn} is the thermoneutral voltage, N_{cell} is the number of cells in series, and U is the stack voltage.

The hydrogen production rate (mol s^{-1}) of an electrolyzer stack is linearly proportional to the stack current

$$\dot{n}_{H_2} = \eta_F N_{cell} \frac{i}{z F}, \tag{3}$$

where z is the number of moles of electrons transferred in the reaction (for hydrogen, $z = 2$), F is the Faraday constant (9.6485×10^4 C mol^{-1}), i is the stack current (A), and η_F is the Faraday efficiency, also known as the current efficiency, and N_{cell} is the number of electrolytic cells in series.

The specific energy consumption E_s of an electrolysis process can be obtained based on the stack voltage, current, and hydrogen production rate

$$E_s = \frac{\int_0^T i(t)\, u(t)\, dt}{\int_0^T \dot{m}_{H_2}\, dt}, \tag{4}$$

where T is the time interval under study. The higher heating value (HHV) is the minimum energy required to produce hydrogen gas with a thermoneutral process. The per mass unit HHV of hydrogen gas is 39.4 kWh kg^{-1}, which can be assumed to represent the energy consumption of the process with a 100% energy efficiency.

3. Results and discussion

The following section presents the main results of in situ water electrolyzer stack performance. First, an improvement of the electrolyte flow with computational fluid dynamics tools is mentioned. Subsequently, values of Faraday efficiency and specific energy consumption are calculated based on hydrogen production rates. Finally, substantial performance enhancement by electrode surface modification is described in detail.

3.1. Improvement of the electrolyte flow

The geometry of the electrolyzer stack was designed by using computational fluid dynamics (CFD) to avoid a stagnated flow and to achieve a revolving flow in laminar flow conditions. A widely used and extensively validated OpenFOAM (openfoam.org) library was used as the CFD software. Even though the desired flow situation was a laminar flow, a detached eddy simulation (DES) turbulence modeling procedure was applied. The k-ω SSTDES (Menter et al., 2003) model (Shear Stress Transport DES) was used as a turbulence model for the simulation. In the DES procedure, the core region of the flow is simulated using large eddy simulation (LES), and in the vicinity of the wall, the traditional RANS (Reynolds Averaged Navier Stokes) turbulence model is used. By this method, excessive computational resources are not needed unlike in the case of a real LES simulation because of the dense grid resolution requirement in the boundary layer region. When the flow velocity is slow enough and the flow approaches the laminar case, excessive dissipation produced by the subgrid model of the DES ceases, and the simulation is a laminar simulation in effect. The computational grids used in the simulation consist of about 1 million cells. Because of the large number of geometries tested and the time-dependent nature of the DES simulation, relatively coarse meshes were used.

Design exploration was used to find a suitable geometry; some of the designs investigated are presented in Fig. 3. The preliminary geometry produced stagnation flow, and therefore, several geometry variations were tested and simulated further. The final geometry was visualized by CFD simulation to produce uniform flow velocity distribution. The resulting flow geometry is asymmetric and enables uniform flow in laminar flow conditions. It should be noted that a mathematical optimization algorithm was not used, and it was left for a future study.

3.2. In situ hydrogen production

First, the performance of the electrolyzer stack was verified by measuring the exhaust gas hydrogen content with a binary gas analyzer under air flush with a constant flow of 5 L min^{-1}. The performance was compared for both a serial and a parallel connection of 5 electrolyzer stack cells. In case of serial connection the stack voltage is the sum of cell voltages as in parallel connection the stack current is the sum of cell

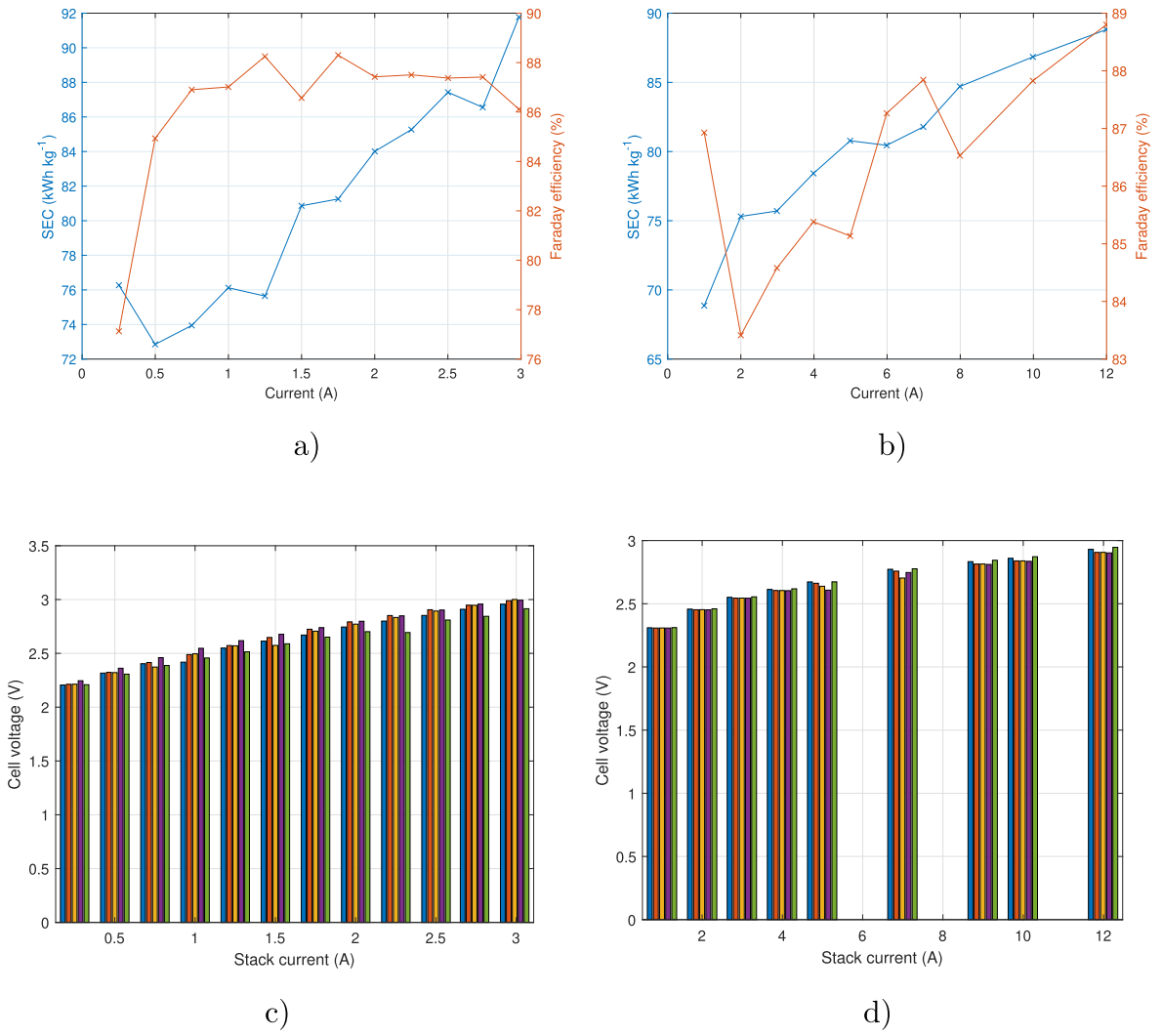

Fig. 4. Specific energy consumption (SEC) and Faraday efficiency as a function of stack current for (a) serial connection and (b) parallel connection of 5 electrolyzer stack cells; Example of individual cell voltages distribution of the in situ water electrolyzer stack as a function of stack current for (c) serial connection and (d) parallel connection.

currents. The specific energy consumption (SEC) and Faraday efficiency of the stack were calculated based on the collected current–voltage relationships and the measured hydrogen production and presented in Fig. 4.

The previous stack prototype (Ruuskanen et al., 2021) suffered from high leakage currents as maximum Faraday efficiency with serial connection was around 50%. In the newer version leakage currents were decreased by applying an insulating Teflon coating throughout the surface of the electrolyzer stack plates except the active electrode area located in the middle. The performance of the solution was verified by the evenly distributed cell voltages in the stack for both the parallel and serial connections as it is depicted in Fig. 4c and in Fig. 4d. In both cases, the Faraday efficiency was close to 90% at cell currents of 1.5 A–2.5 A indicating that leakage currents are relatively small. The hydrogen production rate was almost similar for both serial and parallel connection of the stack cells. For instance, at stack current of 2 A and stack voltage of 15.17 V the hydrogen production rate was 3.66 NL h^{-1} and at 10 A and 2.89 V it was 3.68 NL h^{-1}, correspondingly for serial and parallel connection.

Furthermore, the specific energy consumption was significantly reduced in contrast with the earlier study despite the use of the PBS with a lower conductivity (Ruuskanen et al., 2021). As the cell voltages are at the same range compared with the previous stack prototype the performance improvement is mainly because of the reduced leakage currents. For the current range of 1.5 A–2.5 A per cell, the specific energy consumption did not exceed 90 kWh kg_{H2}^{-1}, which, once again, indicates successful redesign of the electrolyzer stack with the application of proper insulation. The obtained values of SEC are almost 1.8 times as high as that of the traditional alkaline and PEM electrolyzers, which are typically around 50 kWh kg_{H2}^{-1} at 47% – 82% efficiency (Ursúa et al., 2012). One of the factors leading to higher SEC even under Faraday efficiencies of 90% is lower conductivity of PBS solution in comparison to, for instance, KOH used in alkaline water electrolysis. However, it is evident that despite certain similarities between pH-neutral in situ water electrolysis and conventional water electrolysis, the application of these technologies varies significantly. Thus, it is not fair to give any negative conclusions regarding the viability of the studied process based only on efficiency and SEC differences (Rieth and Nocera, 2020).

3.3. Modification of the electrolyzer stack surface and performance evaluation

In order to further enhance the performance of the electrolyzer stack, different surface modification options were examined. First, coating with the benchmark Co–Pi catalysts deposited onto a polished stainless steel electrode plate was tested. Amid deposition of Co–Pi, a gradual

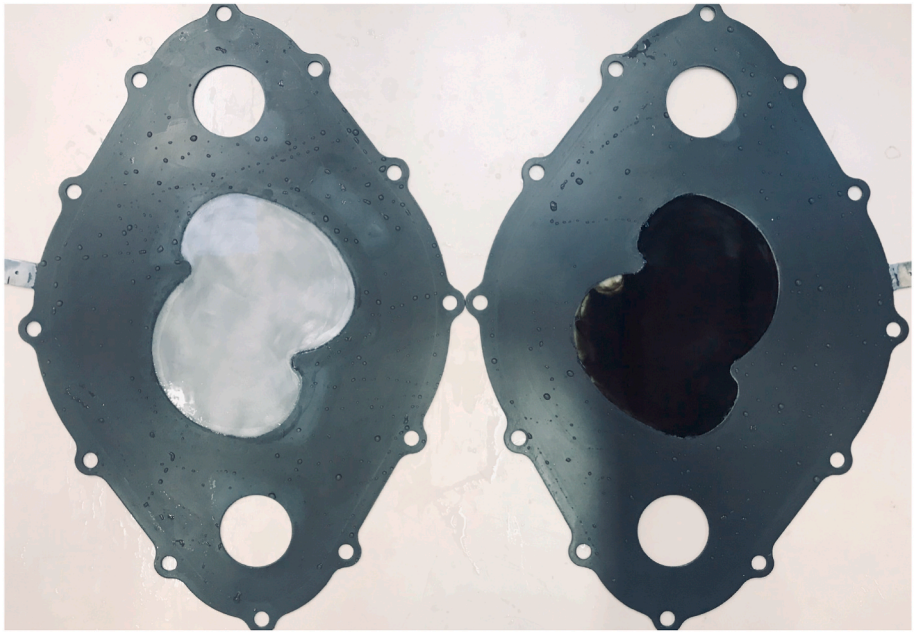

Fig. 5. Photo of the electrolyzer stack plates before and after coating with the CoPi catalyst.

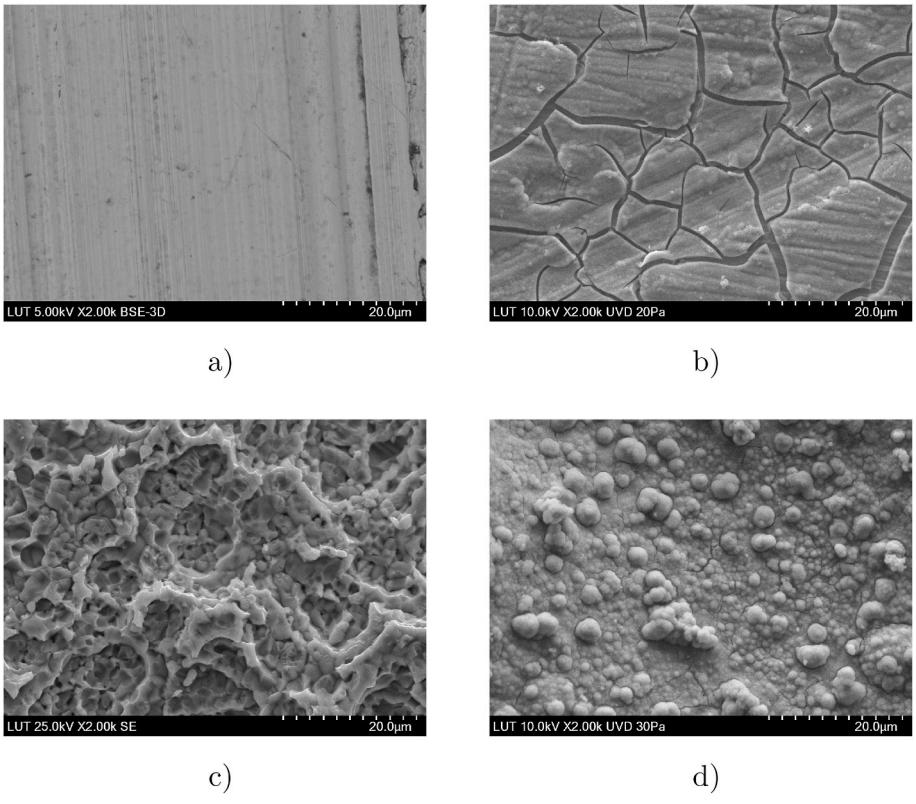

Fig. 6. SEM images of (a) bare SS, (b) Co-Pi on SS, (c) etched SS, and (d) CoFe–P on the etched SS at the same magnification.

increase in the voltammetric current was observed, indicating a higher coverage of the substrate surface and an increasing thickness of the coating. After deposition of Co–Pi, the active area of all the anode plates was evenly coated with a dark coating as shown in Fig. 5. As expected, all the cathode plates remained uncoated.

After deposition and visual inspection, the selected anode plate was analyzed with SEM equipped with EDS. According to Fig. 6b, the flat SS surface (Fig. 6a) was coated with numerous 3D-porous micrometer-size particles. Based on the EDXA diagram depicted in Fig. 7b, the presence of the desired Co and P was evident. The cracks observed on the surface of Co–Pi are a result of the moisture loss during the drying process.

The performance of the electrolyzer stack was analyzed with LSV before and after coating with Co–Pi in a neutral PBS. For all the LSV measurements, the electrolyzer stack was connected in parallel. As it can be seen in Fig. 7d, before coating there was absolutely no current flow in the electrolyzer stack until the potential reached 2.15 V. After 2.15 V,

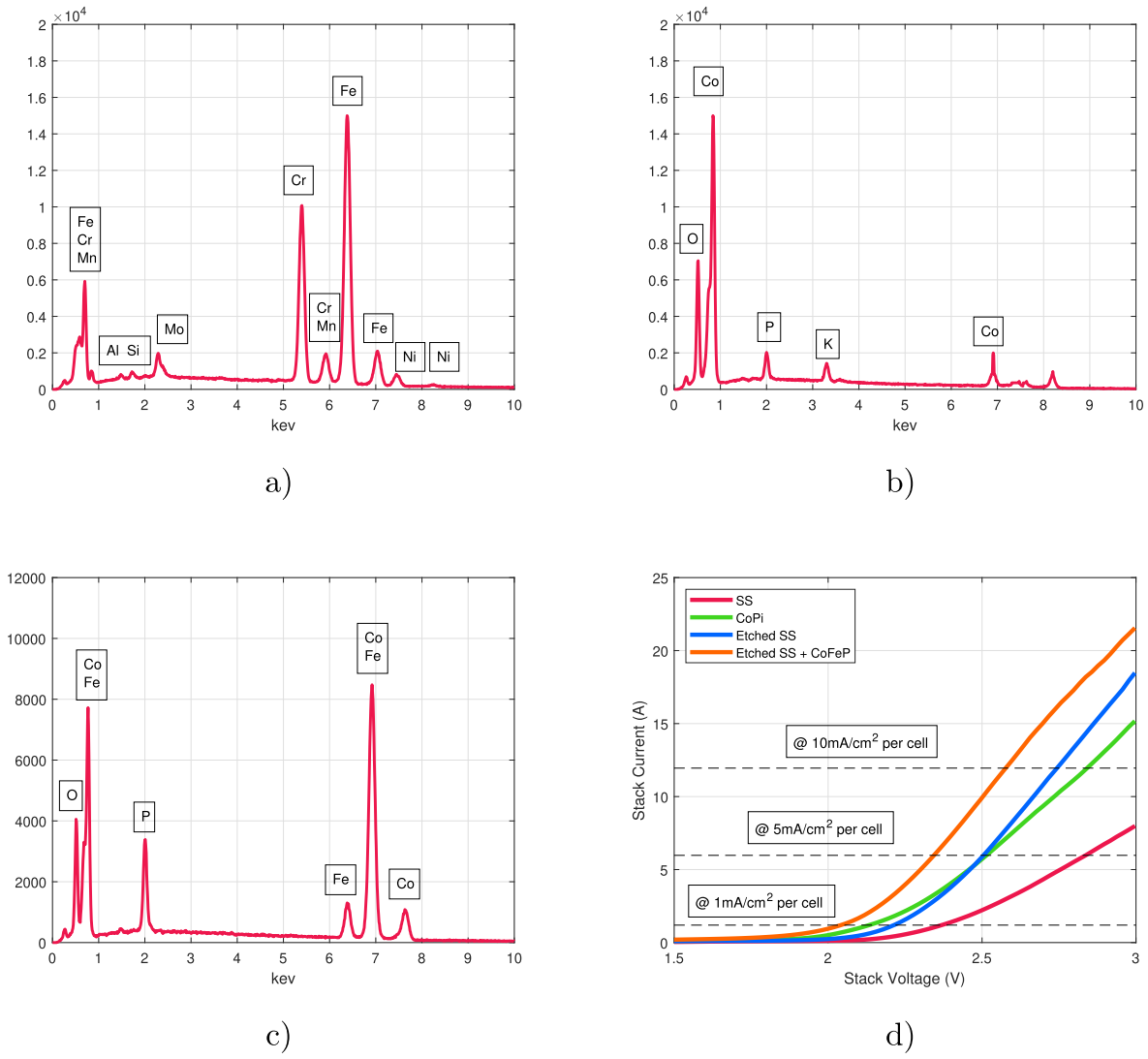

Fig. 7. EDXA spectra for (a) etched SS, (b) CoPi on SS, (c) CoFe–P on SS, and (d) corresponding LSV curves of the electrolyzer stack with different surface morphologies.

the gradual increase in current started to reach the reference current densities of 1 mA cm^{-2} and 5 mA cm^{-2} per electrolyzer cell at the overpotentials of 1.14 V and 1.6 V, respectively. The reference current density of 10 mA cm^{-2} was not reached at 3 V. After coating of the anode plates with Co–Pi, a considerable increase in the electrolyzer stack performance was observed. The current started to rise steeply already after 1.85 V. The same reference current densities of 1 mA cm^{-2} and 5 mA cm^{-2} were reached at significantly lower overpotentials of 0.9 V and 1.28 V in comparison with the bare SS anodes.

In the present study, etching with a mixture of H_2O_2 and HCl was used to roughen the substrate surface and to bare the grains of stainless steel. One can see in Fig. 6c that by that means, the active surface area of the electrolyzer stack plates has been significantly increased. The effect of etching on the electrolyzer stack performance was studied with the LSV, and it is illustrated in Fig. 7d. After 2 V, the current in the etched electrolyzer stack started to rise steeply, reaching a current density of 5 mA cm^{-2} per electrolyzer cell at a similar overpotential of 1.28 V as in the case of the anodes coated with Co–Pi. Although before 2.5 V the performance of the stack was slightly worse compared with the previous test with the Co–Pi coating, after 2.5 V the current rise in the etched stack was faster. The maximum current achieved at 3 V in the etched stack was close to 18 A, which is approximately 3 A higher than that of the electrolyzer stack coated with Co–Pi.

After experiments with etched SS surfaces, another CoFe–P-based coating was tested for the electrolyzer stack because of the high catalytic activity reported in the previous studies (Li et al., 2019; Yoon et al., 2018). During deposition of the CoFe–P catalyst, a gradual decrease in the potential region of the HER was observed. At the end of the deposition procedure, the selected plate was checked once again with SEM equipped with EDS, which revealed a clear change in the surface morphology (Fig. 6d) and the presence of the desired Co, Fe, and P peaks in the diagram (Fig. 7c). The CoFe–P morphology is presented with nodular grains covered with nanoparticles, which explains the large specific surface area and the high catalytic activity of this coating. Similar to the previous reports (Kanan and Nocera, 2008; Yoon et al., 2018), the XRD diffraction peaks of both the tested Co-based coatings revealed the amorphous nature of the synthesized catalysts.

It appeared that with the CoFe–P coating deposited onto the etched SS anodes, the onset overpotential was the lowest, and all the reference current densities were reached at lower overpotentials among all the previously tested options. The current started to increase rapidly before the potential in the stack reached 1.75 V, indicating the start of water splitting. Subsequently, the reference current densities of 1 mA cm^{-2}, 5 mA cm^{-2}, and 10 mA cm^{-2} per electrolyzer cell were reached at the overpotentials of 0.8 V, 1.07 V, and 1.34 V, respectively. At 3 V, the current in the electrolyzer etched and coated with CoFe–P was 2.7 times

as high as in the configuration with flat and uncoated SS electrodes. The superior performance is due to both the increased active surface area achieved by etching and the high intrinsic catalytic effect of the CoFe–P coating in neutral pH.

4. Conclusions

In the present study, a novel pilot-scale in situ water electrolyzer stack for HBI systems was designed and tested. The specific energy consumption and Faraday efficiency of the developed electrolyzer were reported. Compared with the previous research, the performance of the in situ water electrolyzer was considerably enhanced. Above all, leakage currents were prevented by the successful implementation of the insulating Teflon coating. Secondly, the use of modern fluid dynamics tools enabled the improvement of the electrolyte flow. Finally, modification of the active electrode surface area by applying a combination of etching and deposition of in situ Co–Fe–P-based electrocatalysts allowed to reach enhanced current densities at similar voltages in the stack. The results achieved in the study could be considered another crucial step in the development and upscaling of the HBI process.

CRediT authorship contribution statement

Georgy Givirovskiy: Conceptualization, Methodology, Investigation, Validation, Writing – original draft. **Vesa Ruuskanen:** Conceptualization, Methodology, Software, Investigation, Writing – original draft, Project administration, Funding acquisition. **Petteri Kokkonen:** Conceptualization, Methodology, Investigation, Writing – original draft. **Aku Karvinen:** Conceptualization, Methodology, Investigation, Writing – original draft. **Daria Givirovskaia:** Investigation, Writing – review & editing. **Eveliina Repo:** Resources, Writing – review & editing. **Jero Ahola:** Conceptualization, Methodology, Resources, Writing – review & editing, Funding acquisition, Supervision.

Declaration of competing interest

The authors declare that they have no known competing financial interests or personal relationships that could have appeared to influence the work reported in this paper.

Acknowledgment

This work was supported by the Academy of Finland [grant numbers 295883, 295866]; the Technology Industries of Finland Centennial Foundation with Jane and Aatos Erkko Foundation [grant "Feed and food from carbon dioxide and electricity–research and piloting of the future protein production."]

References

Alattar, A.L., Bazhin, V.Y., 2020. Al–Cu–B_4C composite materials for the production of high-strength billets. Metallurgist 64, 566–573. https://doi.org/10.1007/s11015-020-01028-2.

Bhandari, R., Trudewind, C.A., Zapp, P., 2014. Life cycle assessment of hydrogen production via electrolysis - a review. J. Clean. Prod. 85, 151–163. https://doi.org/10.1016/j.jclepro.2013.07.048.

De Francesco, M., Costamagna, P., 2004. On the design of electrochemical reactors for the treatment of polluted water. J. Clean. Prod. 12, 159–163. https://doi.org/10.1016/S0959-6526(02)00191-9.

Geissdoerfer, M., Savaget, P., Bocken, N.M., Hultink, E.J., 2017. The Circular Economy – a new sustainability paradigm? J. Clean. Prod. 143, 757–768. https://doi.org/10.1016/j.jclepro.2016.12.048.

Givirovskiy, G., Ruuskanen, V., Ojala, L.S., Kokkonen, P., Ahola, J., 2019. In situ water electrolyzer stack for an electrobioreactor. Energies 12, 1–13. https://doi.org/10.3390/en12101904.

Givirovskiy, G., Ruuskanen, V., Väkiparta, T., Ahola, J., 2020. Electrocatalytic performance and cell voltage characteristics of 1st- row transition metal phosphate (TM-Pi) catalysts at neutral pH. Mater. Today Energy 17, 1–11. https://doi.org/10.1016/j.mtener.2020.100426.

Kanan, M.W., Nocera, D.G., 2008. In situ formation of an oxygen-evolving catalyst in neutral water containing phosphate and Co^{2+}. Sci 321, 1072–1075. https://doi.org/10.1126/science.1162018.

Krieg, T., Sydow, A., Schro, U., Schrader, J., Holtmann, D., 2014. Reactor concepts for bioelectrochemical syntheses and energy conversion. Trends Biotechnol. 32, 645–655. https://doi.org/10.1016/j.tibtech.2014.10.004.

Li, K., Li, Y., Peng, W., Zhang, G., Zhang, F., Fan, X., 2019. Bimetallic Iron–Cobalt catalysts and their applications in energy-related electrochemical reactions. Catalysts 9. https://doi.org/10.3390/catal9090762.

Liu, C., Colón, B.C., Ziesack, M., Silver, P.A., Nocera, D.G., 2016. Water splitting–biosynthetic system with CO_2 reduction efficiencies exceeding photosynthesis. Sci 352, 1210–1213. https://doi.org/10.1126/science.aaf5039.

Liu, C., Colón, B.E., Silver, P.A., Nocera, D.G., 2018. Solar-powered CO_2 reduction by a hybrid biological | inorganic system. J. Photochem. Photobiol. Chem. 358, 411–415. https://doi.org/10.1016/j.jphotochem.2017.10.001.

Menter, F.R., Kuntz, M., Langtry, R., 2003. Ten years of industrial experience with the SST turbulence model turbulence heat and mass transfer. Cfd.Spbstu.Ru 4, 625–632.

Nangle, S.N., Sakimoto, K.K., Silver, P.A., Nocera, D.G., 2017. Biological-inorganic hybrid systems as a generalized platform for chemical production. Curr. Opin. Chem. Biol. 41, 107–113. https://doi.org/10.1016/j.cbpa.2017.10.023.

Nieminen, H., Givirovskiy, G., Laari, A., Koiranen, T., 2018. Alcohol promoted methanol synthesis enhanced by adsorption of water and dual catalysts. J. CO_2 Util. 24, 180–189. https://doi.org/10.1016/j.jcou.2018.01.002.

Nocera, D.G., Nash, M.P., 2006. Powering the planet: chemical challenges in solar energy utilization. PNAS 103, 15729–15735. https://doi.org/10.1073/pnas.0603395103.

Osadolor, O.A., Lennartsson, P.R., Taherzadeh, M.J., 2014. Introducing textiles as material of construction of ethanol bioreactors. Energies 7, 7555–7567. https://doi.org/10.3390/en7117555.

Rieth, A.J., Nocera, D.G., 2020. Hybrid inorganic-biological systems: faradaic and quantum efficiency, necessary but not sufficient. Joule 4, 2051–2055. https://doi.org/10.1016/j.joule.2020.08.012.

Ruuskanen, V., Givirovskiy, G., Elfving, J., Kokkonen, P., Karvinen, A., Järvinen, L., Sillman, J., Vainikka, M., Ahola, J., 2021. Neo-Carbon Food concept : a pilot-scale hybrid biological inorganic system with direct air capture of carbon dioxide. J. Clean. Prod. 278, 1–11. https://doi.org/10.1016/j.jclepro.2020.123423.

Szczygieł, J., Kułażyński, M., 2020. Thermodynamic limitations of synthetic fuel production using carbon dioxide: a cleaner methanol-to-gasoline process. J. Clean. Prod. 276 https://doi.org/10.1016/j.jclepro.2020.122790.

Torella, J.P., Gagliardi, C.J., Chen, J.S., Bediako, D.K., Colón, B., Way, J.C., Silver, P.A., Nocera, D.G., 2015. Efficient solar-to-fuels production from a hybrid microbial-water-splitting catalyst system. Proc. Natl. Acad. Sci. Unit. States Am. 112, 2337–2342. https://doi.org/10.1073/pnas.1424872112.

Ursúa, A., Gandía, L., Sanchis, P., 2012. Hydrogen production from water electrolysis: current status and future trends. Proc. IEEE 100, 410–426. https://doi.org/10.1109/JPROC.2011.2156750.

Wrana, N., Sparling, R., Cicek, N., Levin, D.B., 2010. Hydrogen gas production in a microbial electrolysis cell by electrohydrogenesis. J. Clean. Prod. 18, S105–S111. https://doi.org/10.1016/j.jclepro.2010.06.018.

Xing, J., Li, H., Cheng, M.M.c., Geyer, S.M., Ng, K.Y.S., 2016. Electro-synthesis of 3D porous hierarchical Ni – Fe phosphate film/Ni foam as a high-efficiency bifunctional electrocatalyst for overall water splitting. J. Mater. Chem. 4, 13866–13873. https://doi.org/10.1039/c6ta05952j.

Yoon, S., Kim, J., Lim, J.H., Yoo, B., 2018. Cobalt iron-phosphorus synthesized by electrodeposition as highly active and stable bifunctional catalyst for full water splitting. J. Electrochem. Soc. 165, H271–H276. https://doi.org/10.1149/2.1221805jes.

Zhang, W., Zhang, F., Niu, Y., Li, Y.X., Jiang, Y., Bai, Y.N., Dai, K., Zeng, R.J., 2020. Power to hydrogen-oxidizing bacteria: effect of current density on bacterial activity and community spectra. J. Clean. Prod. 263, 121596. https://doi.org/10.1016/j.jclepro.2020.121596.